Mathematical Biosciences and Engineering

MBE, 18(3): 1966–1980.
DOI: 10.3934/mbe.2021102
Received: 06 November 2020
Accepted: 17 February 2021
Published: 25 February 2021

http://www.aimspress.com/journal/MBE

Research article

FFT-based equal-integral-bandwidth feature extraction of vibration signal of OLTC

Rongyan Shang*, Changqing Peng, Pengfei Shao and Ruiming Fang

College of Information Science and Engineering, Huaqiao University, Xiamen 361021, China

* **Correspondence:** Email: Shangry@hqu.edu.cn.

Abstract: This study aimed to propose an equal-integral-bandwidth feature extraction method based on fast Fourier transform (FFT) to solve the problem of cumbersome processing and a large amount of calculation in the common feature extraction algorithm for vibration signals of on-load tap changer (OLTC). First, the vibration signals of OLTC were preprocessed in segments, which highlighted the status features and avoided the shortcomings of the FFT spectrum that lacked time axis information. Second, the vibration signal segments were analyzed with FFT, and the generated signal spectrum was divided into several segments according to equal integral. The bandwidth coefficient obtained in each segment was the characteristic value. Third, this study proposed that adding appropriate time domain features and further improving the algorithm could improve the accuracy of fault diagnosis. Finally, the main mechanical faults of OLTC were simulated, and the vibration signals were collected to carry out the fault diagnosis experiment of OLTC. The results showed that the FFT-based equal-integral-bandwidth feature extraction method was simple in processing, small in calculation, easy to implement in an embedded system, and had a high accuracy of fault diagnosis.

Keywords: equal-integral-bandwidth; fault diagnosis; feature extraction; OLTC; vibration signal

1. Introduction

An on-load tap changer (OLTC) is one of the most error-prone parts in the transformer. When a fault occurs, it threatens the safe and stable operation of the power transformer [1]. OLTC failure is one of the leading causes of high-voltage power transformer failure [2]. Statistics show that transformer accidents caused by OLTC account for more than 20%, and they are mainly mechanical

faults [3,4]. The mechanical fault diagnosis based on vibration analysis can be used for online monitoring and fault diagnosis of the internal mechanical state of the OLTC without stopping or disassembling. This not only greatly improves the work efficiency of maintenance personnel and the accuracy of fault diagnosis, effectively reducing the power outage time of the equipment, but also makes it possible to find faults in the early stage, prevents problems before they occur, and greatly reduces the economic losses caused by accidents. Some companies at home and abroad have adopted vibration signal analysis to monitor the operation status of power transformer OLTC online [5].

The vibration signal of OLTC measured on-site is generally severely disturbed, contains a large amount of interference noise components, and has great time-varying and nonstationary properties. Therefore, accurate extraction of effective features for mechanical fault diagnosis is difficult [6]. How to effectively extract the features of vibration signals of OLTC and improve the accuracy of fault diagnosis are research hotspots. The fast Fourier transform (FFT) method is convenient [7] and has been commonly used in condition monitoring of rotating machinery [8]. However, it has certain problems, such as lack of time- and frequency-positioning functions, difficulty in responding to changes in frequency behavior over time, and conflicts in the resolution of time domain and frequency domain [9]. Wavelet analysis is used in the analysis of vibration signals in OLTC [10]. Duan et al. [11] decomposed the mechanical vibration signal of OLTC by wavelet packet transform and effectively achieved OLTC mechanical vibration signal multiband separation. Gao et al. [12] proved that wavelet packet energy entropy could effectively characterize the frequency composition information of vibration signals of OLTCs at different scales and describe the dynamic characteristics contained in vibration signals on the basis of decomposing the mechanical vibration signals of OLTCs. Wavelet analysis has the disadvantages of energy leakage and non-adaptiveness [13]. Empirical mode decomposition (EMD) is very suitable for processing nonlinear and nonstationary vibration signals [14–16]. Duan et al. [17,18] proposed a multiple-frequency EMD method and a narrowband noise-assisted multivariate EMD method to diagnose the typical mechanical faults of OLTC, which could effectively restrain the aliasing effect and improve the precision. Xu et al. [19] established a Volterra model for the mechanical state of OLTC based on time—frequency characteristics obtained using the ensemble EMD algorithm, which not only solved the nonstationary problem of signals but also greatly relieved the computational complexity and improved the computing speed. Liu et al. [20] applied the variational mode decomposition to the decomposition of an OLTC mechanical vibration signal, which effectively avoided the phenomenon of modal aliasing and enhanced the accuracy of feature extraction. Wang et al. [21] successfully extracted the characteristic frequency of the denoising signal through Hilbert–Huang transform (HHT). Duan et al. [22] presented the combination of an optimized HHT algorithm and Lorentz Information Measure to analyze the vibration signals of OLTC during contact switch. Li et al. [23] obtained a discrete observation vector of the vibration signals for the studied OLTC mechanism, which participated in the hidden Markov model training as the feature vector. Wang et al. [24] applied the Bayes estimation and singular value decomposition to extract the features of vibration signals of OLTC in the fused high-dimension phase space. Zeng et al. [25] effectively extracted the characteristics of OLTC according to the phase space distribution of vibration signals.

On the one hand, the current various feature extraction algorithms have complex principles, cumbersome processing, and large amounts of calculation. When using a mid-high-performance computer for processing, not much pressure exists except for the slightly poor real-time performance. However, if an embedded system is adopted, the threshold for programming is very high and the processing speed cannot meet the real-time requirements [26,27].

On the other hand, the development of the Internet of Things in Electricity also puts forward new requirements for monitoring and diagnosis systems. In recent years, the Internet of Things has become one of the mainstream high-tech development directions with the rise in network cloud computing technology and edge computing technology. Since March 2019, the State Grid Corporation of China proposed a plan to build a Ubiquitous Internet of Things in Electricity [28]. Balancing of operation of data in the local environment and in the cloud is very important. A large amount of basic collected data seems unlikely to be stuffed into the cloud for processing and storage; however, if the key feature information cannot be pushed to the cloud, the role of the collected basic data would become weak.

The requirements for miniaturization, distribution, and low power consumption of equipment have increased with the wide range of application scenarios of online monitoring and intelligent diagnosis systems, a fact that cannot be ignored.

Therefore, how to simplify the frequency domain feature extraction of vibration signals and improve the accuracy of fault diagnosis were the core objectives of this study. After in-depth theoretical research and analysis of a large amount of field-measured data, an FFT-based equal-integral-bandwidth feature extraction method of vibration signals of OLTC was proposed. The rest of this study is organized as follows. In Section 2, the FFT-based equal-integral-bandwidth feature extraction method is discussed in detail. The accuracy and efficiency of the method are validated in Section 3. Finally, conclusions are drawn, and potential areas for future research are highlighted in Section 4.

2. FFT-based equal-integral-bandwidth feature extraction

2.1. Segmented preprocessing of vibration signals of OLTC

Several types of general vibration signal sensors exist, such as displacement sensors, speed sensors, and acceleration sensors. Vibration acceleration reflects the magnitude of impact force, intuitively obtains vibration energy characteristics, and is more suitable for the fault diagnosis of OLTC. In addition, the acceleration sensor should be installed as far as possible in the middle of the top cover of the OLTC to obtain a characteristic vibration signal. The waveform of the vibration signal measured during the normal action of the OLTC is shown in Figure 1.

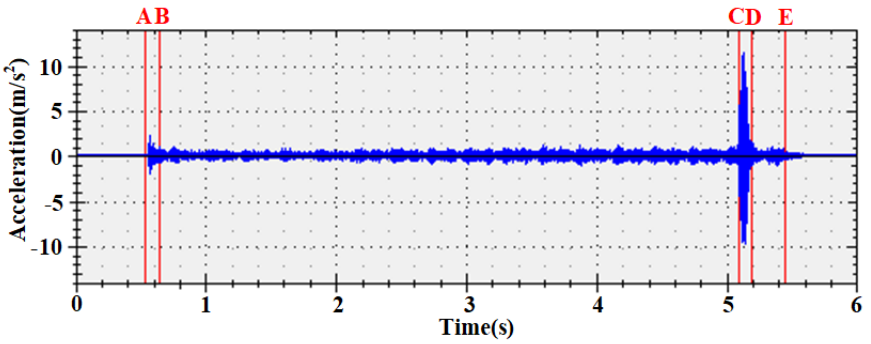

Figure 1. Measured waveform of vibration signal during normal action of OLTC.

Figure 1 shows that the vibration signal of OLTC was unstable in the whole range, including several mutation processes. Therefore, the vibration signal of OLTC was divided into a starting

segment AB, an energy storage segment BC, a switching segment CD, and a stopping segment DE according to the action process.

The starting segment AB and the stopping segment DE had a short time, and the signal was very random. Effectively extracting fault characteristic information and causing interference problems were difficult and usually not used for analysis.

The time of energy storage segment BC was relatively long, and the signal was relatively stable. The switching segment CD was a sudden change in waveform with a wide frequency domain distribution. These two segments were suitable for vibration analysis. Figure 2 shows that the spectral amplitudes of the energy storage segment and the switching segment were very different, and the non-segmented processing obliterated the frequency domain characteristics of the switching segment. Missing the judgment of the faults that mainly occurred in the switching segment was easy.

Therefore, preprocessing the vibration signal in segments to effectively extract the fault feature information was necessary. The vibration signal segmentation was realized by computer calculation, and the vibration signals of the energy storage segment BC and the switching segment CD were separately extracted. The signal characteristics were extracted separately, which was more conducive to accurate fault identification.

Compared with FFT, wavelet packet decomposition (WPD) and EMD had the biggest advantage of not only containing spectrum information but also retaining time axis information. After preprocessing the vibration signal of OLTC in segments, it was approximately regarded as a stable signal for the energy storage segment BC, independent of the time axis information. The signal was thought of as a point on the total time axis for the switching segment CD and was no longer sensitive to time axis information, since the duration was only 1–3.5% of the total duration. Therefore, if the vibration signal was preprocessed in segments, it could perfectly avoid the shortcomings of the FFT spectrum lacking time axis information.

2.2. Vibration signal analysis with FFT

Considering the discrete signal of vibration acceleration in the time domain was $x(n)$, n = 0, 1, 2, …, $N-1$, $N = 2^M$, M = 0, 1, 2, …, $x(n)$ was divided into two groups according to parity, as shown in Eq (2.1) [29].

$$\left.\begin{aligned} x_1(r) &= x(2r) \\ x_2(r) &= x(2r+1) \end{aligned}\right\} \tag{2.1}$$

where $r = 0, 1, \cdots, N/2-1$

When k is 0, 1, …, $N/2-1$, the FFT of $x(n)$ was as shown in Eq (2.2):

$$X(k) = \sum_{r=0}^{N/2-1} x_1(r)\, W_{N/2}^{rk} + W_N^k \sum_{r=0}^{N/2-1} x_2(r) W_{N/2}^{rk} \tag{2.2}$$

where $W_{N/2}^{rk}$ is the twiddle factor, $W_{N/2}^{rk} = e^{-j\frac{2\pi rk}{N/2}}$

When k is $N/2$,..., $N-1$, the FFT of $x(n)$ is as shown in Eq (2.3).

$$X(k) = \sum_{r=0}^{N/2-1} x_1(r)\, W_{N/2}^{rk} - W_N^k \sum_{r=0}^{N/2-1} x_2(r) W_{N/2}^{rk} \tag{2.3}$$

The sampling frequency of the vibration signal was f_s, and the number of sampling points was N. After FFT, the frequency of a certain point n was as shown in Eq (2.4):

$$f_n = n \cdot f_s / N \tag{2.4}$$

The vibration signal $x(n)$ was transformed by FFT to get $X(k)$, and the form of $X(k)$ was a complex number. Its modulus divided by $N/2$ gave the signal amplitude $Y(n)$ at the corresponding frequency (for a direct current (DC) signal, it was divided by N), and its phase was the signal phase at the corresponding frequency.

The vibration signals of the energy storage segment and the switching segment of OLTC were analyzed with FFT, and the generated frequency spectrum is shown in Figure 2.

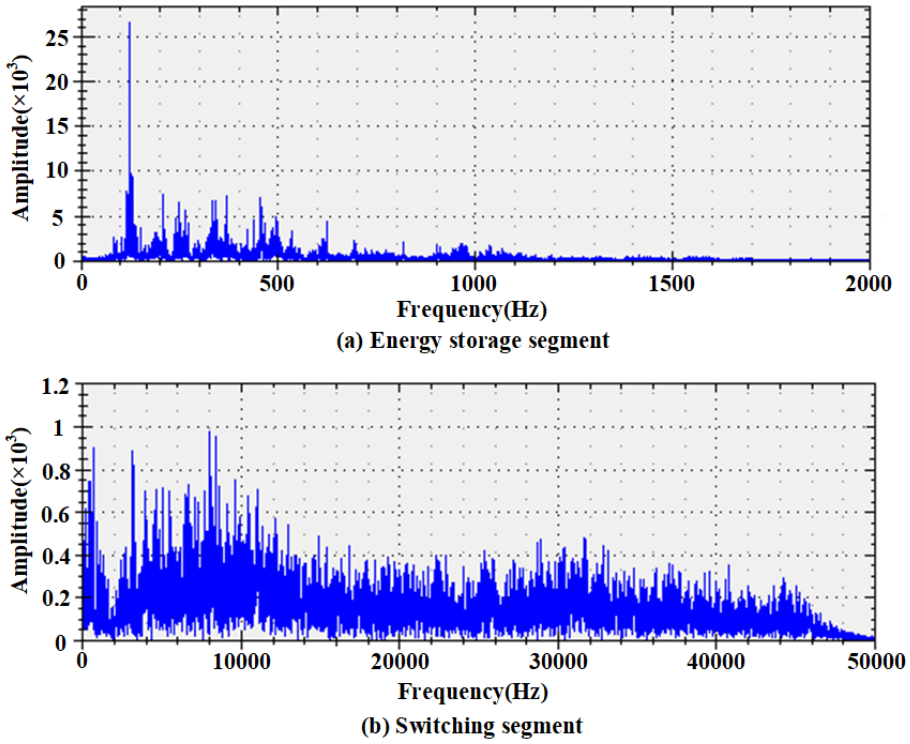

Figure 2. Vibration signal spectrum of OLTC.

2.3. Equal-integral-bandwidth feature extraction

The signal FFT spectrum amplitude $Y(n)$ was integrated after the preprocessing of the segment, and the integral sum and σ were obtained as shown in Eq (2.5).

$$\sigma = \sum_{n=0}^{N-1} Y(n) \tag{2.5}$$

The number of segments was set to m; then, the integral sum of each segment was as shown in Eq (2.6):

$$\sigma' = \sigma / m \tag{2.6}$$

$Y(n)$ was divided into m segments according to the amplitude integral of each segment, which equaled σ', and the bandwidth $b(i)$ of each segment was found (where $i = 1, 2, ..., m$). The bandwidth

coefficient after normalization was calculated as shown in Eq (2.7).

$$b^*(i) = \frac{b(i)}{\sum b(i)} \tag{2.7}$$

The advantage of the FFT-based equal-integral-bandwidth feature extraction of the frequency domain signal was that dividing the bandwidth was no longer an issue. Only by specifying the number of segments, the bandwidth could be adaptively divided and the feature value could be extracted. This method was simple in principle, simple in processing, relatively small in a calculation, and easy to be implemented in various embedded systems.

In summary, the processing flow of the FFT-based equal-integral-bandwidth feature extraction of vibration signals of OLTC is shown in Figure 3.

Figure 3. Processing flow of the vibration signals of OLTC.

2.4. Adding time domain features

In a practical fault diagnosis system, obtaining an ideal recognition accuracy using only frequency domain features was difficult. Some time domain features were added to improve the diagnosis accuracy. According to practical application experience, the frequency domain characteristics of the vibration signals were the main, supplemented by the time domain characteristics of the vibration signal, drive motor current signal [30], acoustic signal, arcing signal [31], and drive shaft angle signal [32], which could achieve a very high recognition rate.

When analyzing the data in this study, no signals other than the vibration signal were introduced, but only some time domain parameters of the vibration signal were introduced as auxiliary criteria, to simplify the analysis. Several commonly used time domain feature values are shown in Eqs (2.8)–(2.10).

Average vibration acceleration: $\bar{V} = \frac{\sum|v_i|}{n}$ (2.8)

Energy consumption index of vibration signal: $E_k = \bar{V} \times T_V$ (2.9)

Standard deviation of vibration signal: $\sigma_V = \sqrt{\frac{\sum(v_i^2)}{n}}$ (2.10)

where v_i is the amplitude of the vibration acceleration curve and T_V is the duration.

It should be noted that if an inappropriate auxiliary criterion is added, the recognition rate decreases to a certain extent.

2.5. Algorithm improvement

According to Section 2.3, for a segment, the larger the spectrum amplitude of the vibration signal, the smaller the normalized bandwidth coefficient $b^*(i)$, indicating to a certain extent that the

frequency weight of the segment was smaller. This was very unfavorable in support vector machines (SVM) training and diagnosis, and the algorithm needed to be improved to change this phenomenon.

The improvement method was to take the natural logarithm of the reciprocal of $b^*(i)$ to obtain the conversion coefficient $b'(i)$ of each segment, as shown in Eq (2.11).

$$b'(i) = ln\frac{1}{b^*(i)} \tag{2.11}$$

The conversion coefficient was normalized again to get the new feature value as shown in Eq (2.12).

$$b'^*(i) = \frac{b(i)}{\sum b\prime(i)} \tag{2.12}$$

After this improvement, further enhancement of the accuracy of fault diagnosis was possible.

3. Experimental procedure

3.1. Sample description

The test object was an OLTC of type CMⅢ 600Y/126C-10193W. The type of the vibration acceleration sensor used was LC0103TB-50. The sampling rate was 100 kSa/s. (The sampling rate of the vibration signal should not be lower than 10 kSa/s, because the main vibration signal spectrum is within 2000 Hz when the OLTC is in action. In addition, considering the limitation of the sensor's frequency range and the pressure of data trans-mission, calculation, and storage, the sampling frequency at this stage is preferably not higher than 100 kSa/s.)

The mechanical faults of OLTC included drive mechanism faults (trip over stop, refusal to move, parts loosening, parts falling off, spindle deformation, jamming, and so forth), switching mechanism faults (spring fatigue, spring breakage, parts loosening, parts falling off, mismatch between groove and wheels, and so forth), and selection mechanism faults (parts loosening, parts falling off, parts distorted and deformed, unbalanced action of the switch, and so forth) [33–37]. Some of these faults were mainly reflected in the energy storage segment, some were reflected in the switching segment, and others affected the whole process.

The OLTC had 17 tap positions, of which 8 up 9, 9 up 10, 10 down 9, and 9 down 8 had transition positions. This study focused only on data without transition position to make the analysis more representative. Excluding upshift 8–9 9–10 and downshift 10–9 9–8, 14 upshifts and 14 downshifts were present (upshift 1–2, 2–3, 3–4, 4–5, 5–6, 6–7, 7–8, 10–11, 11–12, 12–13, 13–14, 14–15, 15–16, and 16–17; downshift 2–1, 3–2, 4–3, 5–4, 6–5, 7–6, 8–7, 11–10, 12–11, 13–12, 14–13, 15–14, 16–15, and 17–16). The continuous samples were measured from upshift 1–2 to upshift 16–17 and then from downshift 17–16 to downshift 2–1. The supplementary samples were obtained by repeated tests of upshift 1–2 and downshift 2–1.

The training samples used upshifts 1–2, 2–3, 3–4, 4–5, 5–6, 12–13, 13–14, 14–15, 15–16, and 16–17 and downshifts 2–1, 3–2, 4–3, 5–4, 6–5, 13–12, 14–13, 15–14, 16–15, and 17–16 in the continuous samples. The extended samples used the supplementary samples, upshifts 6–7, 7–8, 10–11, and 11–12, and downshifts 7–6, 8–7, 11–10, and 12–11. In addition, this experiment did not consider the situation where multiple faults occurred together for the time being. Therefore, spring fatigue + contact wear was only used as the extended sample. As long as the diagnosis result was spring fatigue

or contact wear, the diagnosis was considered correct.

The established samples are shown in Table 1.

The description of fault type in Table 1 is shown in Table 2.

Table 1. Established samples.

Fault code	Fault type	Number of continuous samples	Number of supplementary samples	Number of training samples	Number of extended samples
0	Normal (1)	28	0	20	8
	Normal (2)	28	0	20	8
	Normal (3)	28	6	20	14
1	Contact wear (1)	28	0	20	8
	Contact wear (2)	28	16	20	24
NA	Spring fatigue + contact wear	28	4	0	32
2	Curved plate falling off	28	0	20	8
3	Curved plate loosening	28	0	20	8
4	Jamming (1)	12	0	10	2
	Jamming (2)	28	10	20	18
5	Abnormal switching	28	0	20	8
6	Contact loosening	28	0	20	8
7	Contact falling off	28	0	20	8
8	Main spring fatigue (1)	28	0	20	8
	Main spring fatigue (2)	28	16	20	24
	Total	404	52	270	186

3.2. Horizontal comparison of algorithms

Looking at the vibration state monitoring systems at home and abroad, despite some progress made in various aspects over the years, not many monitoring systems can be truly put into practical applications. The condition monitoring and fault diagnosis of OLTC could be realized using appropriate feature extraction methods and with the help of cloud platforms and mature development frameworks. It might be cheap, convenient, efficient, and high in real time, which was convenient for large-scale promotion.

For comparative research, this study used WPD, EMD, and FFT-based equal-integral-bandwidth feature extraction to extract state features, and then used SVM classifier to realize intelligent diagnosis of the mechanical faults of OLTC. The system structure is shown in Figure 4.

Figure 4 shows that the structure of the fault diagnosis system of OLTC based on WPD or EMD was mainly composed of four parts: sensor, slave computer, host computer, and database [38]. Among these, the signals collected by the sensors mainly included vibration signals (three channels), motor current signals (one channel), and spindle angle signals (1 channel). If necessary, auxiliary signal collection sensors such as on-site environmental temperature and humidity could be added. The slave computer adopted an embedded system, which mainly realized signal conditioning, conversion, acquisition, and preprocessing and pre-diagnosis. The host computer mainly performed advanced

calculation, analysis, and diagnosis of data, and realized the interface with the local warning system, the remote dispatching system, and the mobile application (APP) push system as required. The database mainly realized the storage and indexing of related setting parameters, model parameters, and testing data. The fault diagnosis system based on FFT-based equal-integral-bandwidth feature extraction canceled the industrial computer (PC). After collecting the basic data, it was directly stored in the real-time database server (local shared), and the extracted feature data and diagnosis result data were directly pushed to the cloud.

Table 2. Description of fault type.

Fault type	Description
Normal (1) Normal (2) Normal (3)	No fault. Data were obtained on different dates. OLTC was detachable, so the data might be different.
Contact wear (1)	The surface of a group of four moving and static transition contacts was artificially roughened to simulate the fault that the contacts were burned by the arc.
Contact wear (2)	The surface of 16 A-phase moving contacts was artificially roughened to simulate the fault that the contacts were burned by the arc.
Spring fatigue + contact wear	The main spring was shortened by two turns, and the surface of the 16 A-phase moving contacts was artificially roughened.
Curved plate falling off	The entire curved plate of phase A was removed.
Curved plate loosening	The screws of the A-phase curved plate were loosened.
Jamming (1) Jamming (2)	Sawdust was added to the gearbox. Jamming (1) and Jamming (2) were different in the position and quantity of sawdust.
Abnormal switching	The position of the switch was adjusted so that it was offset by a certain angle.
Contact loosening	The pressure spring of the selector switch contact was cut off for one turn.
Contact falling off	One set of three selector switch contacts was removed.
Main spring fatigue (1)	The main spring was shortened by four turns.
Main spring fatigue (2)	The main spring was shortened by two turns.

The WPD method used the DB3 wavelet basis to perform four-layer decomposition, calculated the integral sum of 16 components and the normalization coefficient of each component, and then took the normalization coefficients of the first 8 components as the main SVM input vector. The EMD method decomposed 10 IMF (intrinsic mode function) components to calculate the integral sum and the normalization coefficient of each component, and took the normalization coefficients of first 8 components as the main SVM input vector. The FFT-based equal-integral-bandwidth feature extraction method took the number of segments as $m = 8$, and used the eight normalization bandwidth coefficients as the main SVM input vector. The fault diagnosis test results are shown in Table 3. In Table 3, error meant that a normal sample was diagnosed as a fault, mistake meant that a fault was diagnosed as another fault, and miss meant that a faulty sample was diagnosed as normal. It was noted that if the sample of spring fatigue + contact wear was diagnosed as major spring fatigue or contact wear, the diagnosis result was considered correct.

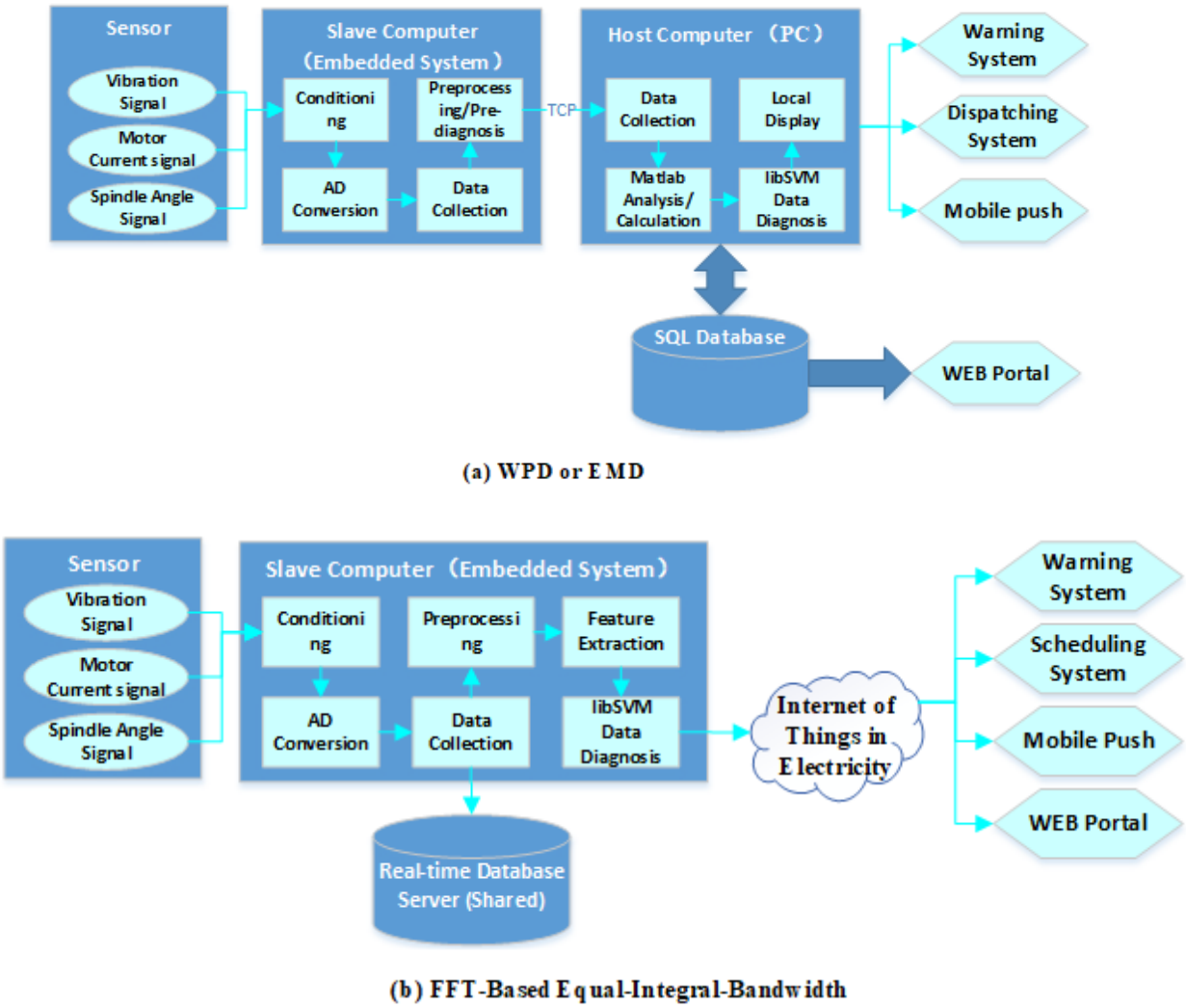

Figure 4. Structure of the fault diagnosis system of OLTC.

Table 3 shows that three methods, including WPD, EMD, and FFT-based equal-integral-bandwidth, were used to extract status features, and then the intelligent fault diagnosis was performed. The diagnostic accuracy of the three was similar, and the FFT-based equal-integral-bandwidth method was even higher.

3.3. Effect of adding time domain features

As shown in Sections 2.3 and 2.4, this study only added the average value of vibration acceleration to simplify the analysis. The diagnostic test results are shown in Table 4.

Tables 3 and 4 show that after adding time domain feature, both the optimal and diagnostic accuracy rates were greatly improved.

It was noted that if an inappropriate auxiliary criterion was added, the recognition rate decreased to a certain extent. For example, using the FFT-based equal-integral-bandwidth method and adding the time domain feature of the maximum vibration acceleration of the switching segment, the optimal accuracy rate greatly reduced to only 71.75%.

Table 3. Diagnosis results.

Fault type	Total number of samples	WPD			EMD			FFT-based equal-integral-bandwidth		
		Error	Miss	Mistake	Error	Miss	Mistake	Error	Miss	Mistake
Normal	90	12		−	12	−	−	7	−	−
Contact wear	72	−		3	−	13	5	−		
Curved plate falling off	28	−		−	−			−		
Curved plate loosening	28	−	5	1	−	2	4	−		
Jamming	50	−		1	−		1	−		
Abnormal switching	28	−	2	3	−	6	4	−	1	3
Contact loosening	28	−	7		−	6	2	−	2	2
Contact falling off	28	−	1		−	2		−	3	
Main spring fatigue	72	−		4	−		6	−	6	12
Spring fatigue + contact wear	32	−	12	4	−	7		−	20	2
Total	456	12	27	24	12	34	22	7	32	19
Optimal accuracy			84.51%			72.54%			88.85%	
Diagnostic accuracy			86.18%			85.09%			87.28%	

Table 4. Diagnostic test results.

	WPD	EMD	FFT-based equal-integral-bandwidth
Optimal accuracy (%)	87.36	76.58	93.68
Diagnostic accuracy (%)	91.22	86.18	95.83

Table 5. Fault diagnosis test results.

Fault type	Total number of samples	Error	Miss	Mistake
Normal	90	2	−	−
Contact wear	72	−		
Curved plate falling off	28	−		
Curved plate loosening	28	−		
Jamming	50	−		
Abnormal switching	28	−	1	
Contact loosening	28	−		
Contact falling off	28	−		
Main spring fatigue	72	−		
Spring fatigue + contact wear	32	−	8	4
Total	456	2	9	4
Diagnostic accuracy		96.71%		

3.4. Effect of improved algorithm

As discussed in Section 2.5, the fault diagnosis test results after improving the FFT-based equal-integral-bandwidth method are shown in Table 5.

Table 5 shows that the diagnostic accuracy rate increased to 96.71%. The main reason for the decrease in diagnostic accuracy was the failure sample of "spring fatigue + contact wear." This confusion could be resolved perfectly when supplemented by the signal characteristics of the current signal. Moreover, the confusion was resolved by putting part of the "spring fatigue + contact wear" fault samples into the training set. However, these aspects were not discussed in detail in this study.

4. Conclusions

This study proposed an equal-integral-bandwidth feature extraction method based on FFT to solve the problem of cumbersome processing and large amount of calculation in the common feature extraction algorithm for the vibration signals of OLTC. The following conclusions were drawn through experimental research:

1) Vibration signals of OLTC were preprocessed in segments, and specific time periods were selected to extract signal features that perfectly avoided the shortcomings of FFT spectrum missing time axis information, highlighted status features, and effectively extracted fault feature information.

2) The energy storage segment and the switching segment of vibration signals of OLTC were selected for FFT analysis. The spectral amplitudes of the two were very different, and the non-segmented processing obliterated the frequency domain characteristics of the switching segment. It was easy to miss the judgment of the faults that mainly occurred in the switching segment.

3) The FFT signal spectrum was segmented by equal integrals, and the bandwidth coefficient obtained from each segment was the feature value. The advantage of the FFT-based equal-integral-bandwidth feature extraction of frequency domain signal was that dividing the bandwidth was no longer an issue. The bandwidth could be adaptively divided and the feature value could be extracted only by specifying the number of segments. By adding appropriate time domain features, the conversion coefficient could be calculated as the feature value, and the correct rate of fault diagnosis could be further improved.

4) The main mechanical failures of OLTC were simulated, vibration signals were collected, and failure diagnosis experiments of OLTC were conducted. The results showed that the FFT-based equal-integral-bandwidth feature extraction method was simple in processing, small in calculation, easy to implement in embedded systems, and had a high fault diagnosis accuracy rate.

This method should be improved in the future to expand its scope of application for its better application to engineering practice. At the same time, future studies should also consider more types of faults, continuously enrich the OLTC mechanical state characteristic database, and further improve the real time and accuracy of OLTC mechanical fault detection.

Acknowledgments

This study was supported in part by the Industry–University Research Project of Xiamen under Project 3502Z20203036 and Project 3502Z20193032 and the Natural Science Foundation of Fujian Province under Project 2012J01223.

Conflict of interest

The authors declare no conflict of interest.

References

1. R. Yang, D. Zhang, Z. Li, K, Yang, S. Mo, L. Li, Mechanical fault diagnostics of power transformer on-load tap changers using dynamic time warping, *IEEE Trans. Instrum. Meas.*, **68** (2019), 3119–3127.
2. F. Riaz, J. Wetzer, A. R. Mor, Innovative approach toward an algorithm for automated defect recognition for on-load-tap changers, *CIRED Open Access Proc. J.*, **2017** (2017), 246–250.
3. X. Zhou, F. H. Wang, J. Fu, J. Lin, Z. Jin, Mechanical condition monitoring of on-load tap changers based on chaos theory and K-means clustering method, *Proc. CSEE*, **35** (2015), 1541–1548.
4. P. J. Kang, D. Birtwhistle, Condition monitoring of power transformer on-load tap-changers. Part I: condition diagnostic, *IEE Proc. Gener. Transm. Distrib.*, **148** (2001), 301–306.
5. J. Seo, H. Ma, T. K. Saha, A joint vibration and arcing measurement system for online condition monitoring of on-load tap changer of the power transformer, *IEEE Trans. Power Delivery*, **32** (2017), 1031–1038.
6. Q. Yang, J. Ruan, Z. Zhuang, Fault diagnosis of circuit breakers based on time–frequency and chaotic vibration analysis, *IET Gener. Transm. Distrib.*, **14** (2020), 1214–1221.
7. G. H. Fan, S. H. Liu, W. D. Liu, L. Wang, Suppression of the periodic narrow-band noise in discharge signal by FFT spectrum minimum entropy deconvolution filtering, *High Voltage Eng.*, **43** (2017), 1378–1385.
8. D. Strömbergsson, P. Marklund, K. Berglund, P. E. Larsson, Bearing monitoring in the wind turbine drivetrain: A comparative study of the FFT and wavelet transforms, *Wind Energy*, **23** (2020), 1381–1393.
9. Z. Zhang, Research on vibration signal analysis and state diagnosis method of transformer on-load tap changer, Ph. D thesis, Chongqing University, Chongqing, 2019.
10. L. Lu, Y. H. Cui, Diagnosis of transformer tap changer contact fault based on vibration signal, *Electr. Power Autom. Equip.*, **32** (2012), 93–97.
11. X. Duan, T. Zhao, T. Li, J. Liu, L. Zou, L. Zhang, Method for diagnosis of on-load tap changer based on wavelet theory and support vector machine, *J. Eng.*, **2017** (2017), 2193–2197.
12. S. Gao, C. Zhou, Z. Zhang, J. Geng, R. He, Q, Yin, et al., Mechanical fault diagnosis of an on-load tap changer by applying cuckoo search algorithm-based fuzzy weighted least squares support vector machine, *Math. Probl. Eng.*, **2020** (2020), 1–11.
13. G. S. Gao, G. L. Yue, C. Zhou, J. Geng, C. Xing, Y. Ding, et al., Applying Hilbert-Huang transform of the Volterra model to diagnosing mechanical fault for on-load tap changer, *High Voltage Appar.*, **56** (2020), 173–180.
14. Y. H. Sun, J. W. Wu, S. J. Lian, L. M. Zhang, Extraction of vibration signal feature vector of circuit breaker based on empirical mode decomposition amount of energy, *Trans. China Electrotech. Soc.*, **29** (2014), 228–236.

15. N. Cai, W. Xie, H. Peng, H. Wang, Z. Yang, X. Chen, A novel error compensation method for an absolute optical encoder based on empirical mode decomposition, *Mech. Syst. Signal Process.*, **88** (2017), 81–88.
16. H. Li, Y. Hu, F. Li, G. Meng, Succinct and fast empirical mode decomposition, *Mech. Syst. Signal Process.*, **85** (2017), 879–895.
17. R. C. Duan, F. H. Wang, Fault diagnosis of on-load tap-changer in converter transformer based on time–frequency vibration analysis, *IEEE Trans. Ind. Electron.*, **63** (2016), 3815–3823.
18. R. C. Duan, F. H. Wang, L. D. Zhou, Mechanical condition detection of on-load tap-changer in converter transformer based on narrowband noise assisted multivariate empirical mode decomposition algorithm, *Trans. China Electrotech. Soc.,* **32** (2017), 182–189.
19. Y. Xu, C. Zhou, J. Geng, S. Gao, P. Wang, A method for diagnosing mechanical faults of on-load tap changer based on ensemble empirical mode decomposition, Volterra model and decision acyclic graph support vector machine, *IEEE Access*, **7** (2019), 84803–84816.
20. J. Liu, G. Wang, T. Zhao, L. Zhang, Fault diagnosis of on-load tap-changer based on variational mode decomposition and relevance vector machine, *Energies*, **10** (2017), 946.
21. C. L. Wang, K. Li, H. Z. Ma, A. Wang, Feature recognition of OLTC vibration signal based on WP_SVD denoising method, *Proc. Chin. Soc. Univ. Electric Power Syst. Autom.*, **24** (2012), 36–41.
22. R. C. Duan, F. H. Wang, L. D. Zhou, Mechanical features extraction of on-load tap-changer in converter transformer based on optimized HHT algorithm and Lorentz information measure, *Proc. CSEE*, **36** (2016), 3101–3109.
23. Q. M. Li, T. Zhao, L. Zhang, J. Lou, Mechanical fault diagnostics of on-load tap changer within power transformers based on hidden Markov model, *IEEE Trans. Power Delivery*, **27** (2012), 596–601.
24. F. H. Wang, Q. H. Zeng, Y. M. Zheng, Y. Qian, A mechanical fault diagnosis of on-load tap-changers based on phase space fusion of Bayes estimation and CM-SVDD, *Proc. CSEE*, **40** (2020), 358–368.
25. Q. H. Zeng, F. H. Wang, Y. M. Zheng, W. He, Fault recognition of on-load tap-changer in power transformer based on convolutional neural network, *Autom. Electric Power Syst.,* **44** (2020), 144–151.
26. J. Lu, M. Zhang, H. F. Zhao, H. Ma, Design of power transformer condition monitoring system based on the vibration signal, *Proc. CSU-EPSA*, **28** (2016),73–77.
27. F. Poza, P. Marino, S. Otero, F. Machado, Programmable electronic instrument for condition monitoring of in-service power transformers, *IEEE Trans. Instrum. Meas.*, **55** (2006), 625–634.
28. *State Grid Corporation of China, White Paper*: Internet of Things in Electricity, 2019. Available from: http://www.199it.com/archives/973655.html.
29. Z. Y. Shen, *MATLAB Signal Processing*, 1st edition, Tsinghua University Press, Beijing, 2017.
30. Z. Li, Q. Li, Z. Wu, J. Wu, R. Zheng, A fault diagnosis method for on load tap changer of aerospace power grid based on the current detection, *IEEE Access*, **6** (2018), 24148–24156.
31. J. Seo, H. Ma, T. K. Saha, On savitzky–golay filtering for online condition monitoring of transformer on-load tap changer, *IEEE Trans. Power Delivery*, **33** (2018), 1689–1698.
32. M. Deng, Min diagnosis of mechanical faults for on-load tap changer based on vibration signal, *Transformer*, **55** (2018), 26–29.

33. M. Chen, H. Z. Ma, Y. Xu, B. B. Chen, H. Xu, L. Wang, Design of monitoring system for on-load tap changer of transformer based on data acquisition card, *Transformer*, **56** (2019), 30–34.
34. K. M. Wang, H. C. Shu, L. P. Cao, J. Dong, Y. G. Su, Study of OLTC running state evaluation method based on correlation analysis, *Power Syst. Prot. Control*, **43** (2015), 54–59.
35. M. Chen, H. Z. Ma, Y. Xu, X. Pan, B. Chen, H. Xu, et al., Mechanical fault diagnosis of on-load tap changer based on empirical mode decomposition algorithm for improved mask signal, *Power Grid Anal. Study*, **47** (2019), 88–94.
36. Z. Y. Liu, H. J. Chen, X. J. Yu, X. Xia, Research progress and prospects on fault diagnosis method for transformer on-load tap changer based on vibration signal, *High Voltage Appar.*, **55** (2019), 18–25.
37. Y. H. Fang, Brief analysis of on-load tap changer faults in transformer, *Transformer*, **48** (2011), 62–65.
38. C. B. Xu, F. H. Wang, J. Fu, J. Lin, Z. Jin, Design and development of vibration test system for power transformer on-load tap changer, *Chin. J. Sci. Instrum.*, **34** (2013), 987–993.

AIMS Press